CHEMISTRY OF MATERIALS
Article

Chem. Mater. **2009,** *21,* 4111–4121 4111
DOI:10.1021/cm8024022

One-Step Preparation of Thiol-Functionalized Porous Clay Heterostructures: Application to Hg(II) Binding and Characterization of Mass Transport Issues

Aurélien Jieumboué Tchinda,[†,‡] Emmanuel Ngameni,[‡] Ignas Tonlé Kenfack,[‡,§] and Alain Walcarius*,[†]

[†]*Laboratoire de Chimie Physique et Microbiologie pour l'Environnement, UMR 7564, CNRS−Université Henri Poincaré Nancy I, 405, Rue de Vandoeuvre, F-54600 Villers-les-Nancy, France,* [‡]*Laboratoire de Chimie Analytique, Faculté des sciences, Université de Yaoundé I, B. P. 812 Yaoundé, Cameroun, and* [§]*Département de Chimie, Faculté des sciences, Université de Dschang, B. P. 67 Dschang, Cameroun*

Received September 5, 2008. Revised Manuscript Received July 12, 2009

Naturally occurring smectite clays have been expanded by a surfactant (cetyltrimethylammonium) and a cosurfactant (dodecylamine), which were then used in combination with the sol−gel process to prepare porous clay heterostructures (PCHs). A variety of thiol-functionalized PCHs have been obtained in one step by surfactant-directed co-condensation of tetraethoxysilane (TEOS) and 3-mercaptopropyltrimethoxysilane (MPTMS) in various molar ratios (ranging from 0 to 35% MPTMS) in the interlayer region of the clay. These materials have been characterized by several physicochemical techniques. They featured large specific surface areas and pore volumes (after template removal), due to the presence of regular mesopore channels between the clay sheets, but the mesostructural order and porosity were found to decrease upon rising the functionalization level. Hg(II) binding to these materials was then analyzed to get insight in the accessibility to the active centers and to characterize mass transfer rates to the binding sites. The experiments have been carried out at two distinct pH values (2 and 4) to point out the influence of speciation on these processes. Full accessibility was always observed at pH 4 where Hg(II) was adsorbed under a neutral form, giving rise to very high sorption capacities (up to about 600 mg g^{-1}). The rate of access to the binding sites was usually faster in the more ordered materials, but some limitations were observed at pH 2 due to unfavorable electrostatic interactions. Finally, hydrodynamic electrochemistry has been applied to demonstrate that mesostructuration of the interlayer region of the clay has positive impact in terms of enhancing diffusion rates through PCH thin films in comparison to nonmodified clay coatings. The layered structure of the materials creates their direct arrangement as mechanically stable layers onto electrode surfaces, contrary to other powdered mesoporous materials which require the use of a polymeric binder.

1. Introduction

Clay minerals have been recognized for a long time as low cost adsorbents due to their ion exchange properties and sorption capacities.[1] A strategy to improve the adsorption capacity and selectivity of clays is the incorporation of organic functionalities exhibiting high affinity and/or preferential recognition properties toward target species like heavy metal ions.[2−5] This can be achieved either by impregnation of organic moieties, which mostly involves the replacement of the native inorganic cations (Ca^{2+}, Na^{+}, and K^{+}) within the clay galleries by organic cations (e.g., quaternary ammonium),[3] by covalent grafting of organic groups onto the surface of layered silicates,[4] or even in one step in the form of organoclay nanocomposites.[5] Such organoclays may however suffer from rather poor accessibility to the binding sites as a result of clogging of the interlayer region of the clay with the organo-functional groups that prevent somewhat the target elements from reaching the active centers in the material.[3b,6] Even pillared clays in which the interlayer region has been expanded[7] can be subject to interlamellar stuffing when grafted with

*E-mail: alain.walcarius@lcpme.cnrs-nancy.fr.

(1) (a) Liu, P.; Zhang, L. X. *Sep. Purif. Technol.* **2007**, *58*, 32. (b) Babel, S.; Kurniawan, T. A. *J. Hazardous Mater.* **2003**, *97*, 219. (c) Bailey, S. E.; Olin, T. J.; Bricka, R. M.; Adrian, D. D. *Water Res.* **1999**, *33*, 2469.
(2) (a) Coelho, A. C. V.; Santos, P. D.; Santos, H. D. *Quim. Nova* **2007**, *30*, 1282. (b) Stathi, P.; Litina, K.; Gournis, D.; Giannopolous, T. S.; Deligiannakis, Y. *J. Colloid Interface Sci.* **2007**, *316*, 298.
(3) (a) Cruz-Guzman, M.; Celis, R.; Hermosin, M. C.; Koskinen, W. C.; Nater, E. A.; Cornejo, J. *Soil. Sci. Soc. Am. J.* **2006**, *70*, 215. (b) Oyanedel-Craver, V. A.; Smith, J. A. *J. Hazardous Mater.* **2006**, *137*, 1102.
(4) (a) Gardênnia da Fonseca, M.; Airoldi, C. *Quim. Nova* **2003**, *26*, 699. (b) Sales, J. A. A.; Petrucelli, G. C.; Oliveira, F. J. V. E.; Airoldi, C. *J. Colloid Interface Sci.* **2006**, *297*, 95. (c) Celis, R.; Hermosin, M. C.; Cornejo, J. *Environ. Sci. Technol.* **2000**, *34*, 4593.
(5) (a) Carrado, K. A. *Appl. Clay Sci.* **2000**, *17*, 1. (b) Jaber, M.; Miehe-Brendle, J.; Michelin, L.; Delmotte, L. *Chem. Mater.* **2005**, *17*, 5275.
(6) (a) Tillman, F. D.; Bartelt-Hunt, S. L.; Craver, V. A.; Smith, J. A.; Alther, G. R. *Environ. Eng. Sci.* **2005**, *22*, 400. (b) Mercier, L.; Detellier, C. *Environ. Sci. Technol.* **1995**, *29*, 1318.
(7) (a) Diaz, M.; Cambier, P.; Brendle, J.; Prost, R. *Appl. Clay Sci.* **2007**, *37*, 12. (b) Bhattacharyya, K. G.; Sen Gupta, S. *Sep. Purif. Technol.* **2006**, *50*, 388. (c) Bouchenafa-Saib, N.; Khouli, K.; Mohammedi, O. *Desalination* **2007**, *217*, 282.

Published on Web 08/18/2009

organo-functional groups because of their microporosity, precluding effective reactivity toward external reagents and leading to, e.g., restricted sorption yields.

A small revolution in that field has merged from the discovery of the so-called "porous clay heterostructures" (PCHs).[8] PCHs are formed by surfactant-directed assembly of mesoporous silica within the galleries of either natural or synthetic clays with 2:1 (mica-type) layered lattice structures, according to a process analogous to that applied to form ordered mesoporous silica particles[9] except that the mesopore channels are not formed in three dimensions but confined in the two-dimensional interlayer region of the clay.[10] This led to highly porous materials after template removal, featuring specific surface areas in the range 300−1000 $m^2\ g^{-1}$ and pore volumes between 0.3 and 0.8 $cm^3\ g^{-1}$. They have been used to date as solid acid catalysts[11] or as adsorbents for organic species.[12] Their catalytic properties can be improved by postsynthesis treatments such as, e.g., grafting of aluminum[13] or copper and iron species.[14]

Organically modified PCHs are less widespread. The first example was described by Mercier and Pinnavaia[15] who have prepared thiol-functionalized adsorbents by grafting the intragallery framework of a PCH with mercaptopropyltrimethoxysilane, and they observed that only 67% of thiol groups was accessible to Hg(II) used as a target probe. It is known from investigations made on functionalized mesoporous silica materials that the grafting process can have some drawbacks in comparison to the direct co-condensation synthetic pathway[16] (amount of organic groups restricted to the specific surface area of the material, preferential grafting at the mesopore entrance and thereby less homogeneous dispersion of these groups in the mesostructure (except if experimental conditions are used to get a self-assembled monolayer of the grafting agent[17a]), loss of porosity upon grafting). Considering that point, it might be surprising that very few works have been directed to date to the preparation of organically functionalized PCHs by such a direct assembly of surfactant-templated organosilica in the galleries of layered clays.[18] In particular, no attempt was made to get adsorbents with increased capacities with respect to grafted PCHs[15] or to improve accessibility to the binding sites or mass transport rates in such porous environments.

The current work describes the preparation of thiol-functionalized PCHs (PCH-SH*n*%) via a one-step method involving the direct co-condensation of tetraethoxysilane (TEOS) and 3-mercaptopropyltrimethoxysilane (MPTMS), at various molar ratios (*n*% up to 35% MPTMS relative to the total amount of precursor), in the intragallery region of natural cameroonian clay. It also shows the effect of the functionalization level on the degree of organization and porosity of the material and discusses the accessibility of Hg(II) species to the binding sites in terms of adsorbent capacity and mass transport rates. The thiol-mercury system has been chosen here at it is well-known in the mesoporous organosilica community (accessibility,[17] kinetics,[19] speciation[20]). Finally, we will also demonstrate how clay-derived heretrostructures can be useful to increase the sensitivity of clay modified electrodes by accelerating the rate-determining step (diffusion through the layer).

2. Experimental Section

Materials and Reagents. All commercially available chemicals were used as received. Tetraethoxysilane (TEOS, 98%) and 3-mercaptopropyltrimethoxysilane (MPTMS, 95%) were purchased from Sigma-Aldrich. Dodecylamine (DDA, 99%) was obtained from Fluka, and cetyltrimethylammonium bromide (CTAB, 98%), from Merck. Solvents; other reagents (HNO_3, HCl, $NaNO_3$, NaOH) were supplied by Riedel-de-Häen or Prolabo. All analytical solutions were prepared with high purity water (18 $M\Omega\ cm^{-1}$) obtained from a Millipore milli-Q water purification system. A standardized stock solution containing Hg^{2+} at 1000 ± 2 mg L^{-1} (Sigma-Aldrich) was used to prepare diluted samples of this analyte. The pristine clay, named "Ba", was collected from the Baba deposits (West-Cameroon, central Africa). It was purified by sedimentation, as described earlier,[21] to recover only the fine fraction (below 2 μm) consisting of low charge montmorillonite with mixed "$Na^+-K^+-Ca^{2+}$" filling characterized by a cation exchange capacity of 0.89 mequiv g^{-1}.[24]

(8) Galarneau, A.; Barodawalla, A.; Pinnavaia, T. J. *Nature* **1995**, *374*, 529.

(9) (a) Kresge, C. T.; Leonowicz, M. E.; Roth, W. J.; Vartuli, J. C.; Beck, J. S. *Nature* **1992**, *359*, 710. (b) Beck, J. S.; Vartuli, J. C.; Roth, W. J.; Leonowicz, M. E.; Kresge, C. T.; Schitt, K. D.; Chu, C. T-W.; Olson, D. H.; Sheppard, E. W.; McCullen, S. B.; Higgins, J. B.; Schlenker, J. L. *J. Am. Chem. Soc.* **1992**, *114*, 10834.

(10) (a) Pinnavaia, T. J.; Galarneau, A.; Barodawalla, A. U. S. Patent 5,726,113, **1998**. (b) Cool, P.; Vansant, E. F. In *Handbook of Layered Materials*; Aurbach, S. M., Carrado, K. A., Dutta, P. K., Eds.; Marcel Dekker, Inc.: New York, 2004; pp 261−311.

(11) (a) Galarneau, A.; Barodawalla, A.; Pinnavaia, T. J. *Chem. Commun.* **1997**, 1661. (b) Polverejan, M.; Pauly, T. R.; Pinnavaia, T. J. *Chem. Mater.* **2000**, *12*, 2698.

(12) (a) Pires, J.; Araujo, A. C.; Carvalho, A. P.; Pinto, M. L.; Gonzalez-Calbet, J. M.; Ramirez-Castellanos, J. *Microporous Mesoporous Mater.* **2004**, *73*, 175. (b) Arellano-Cardenas, S.; Gallardo-Velazquez, T.; Osorio-Revilla, G.; Lopez-Cortez, M. D. *Water Environ. Res.* **2008**, *80*, 60.

(13) (a) Ahenach, J.; Cool, P.; Vansant, E. F . *Phys. Chem. Chem. Phys.* **2000**, *2*, 5750. (b) Polverejan, M.; Liu, Y.; Pinnavaia, T. J. *Chem. Mater.* **2002**, *14*, 2283.

(14) (a) Chmielarz, L.; Kustrowski, P.; Drozdek, M.; Cool, P.; Vansant, E. F. *Catal. Today* **2006**, *114*, 319. (b) Chmielarz, L.; Kustrowski, P.; Dziembaj, R.; Cool, P.; Vansant, E. F. *Catal. Today* **2007**, *119*, 181.

(15) Mercier, L.; Pinnavaia, T. J. *Microporous Mesoporous Mater.* **1998**, *20*, 101.

(16) (a) Lim, M. H.; Stein, A. *Chem. Mater.* **1999**, *11*, 3285. (b) Mercier, L.; Pinnavaia, T. J. *Chem. Mater.* **2000**, *12*, 188. (c) Corriu, R. J. P.; Lancelle-Beltran, E.; Mehdi, A.; Reyé, C.; Brandès, S.; Guilard, R. *J. Mater. Chem.* **2002**, *12*, 1355.

(18) (a) Wei, L.; Tang, T.; Huang, B. *Microporous Mesoporous Mater.* **2004**, *67*, 175. (b) Ferreira, P.; Nunes, C. D.; Pires, J.; Carvalho, A. P.; Brandao, P.; Rocha, J. *Mater. Sci. Forum* **2006**, *514−516*, 470. (c) Jieumboué Tchinda, A.; Ngameni, E.; Walcarius, A. *Sens. Actuators B* **2007**, *113*, 121.

(17) (a) Feng, X.; Fryxell, G. E.; Wang, L.-Q.; Kim, A. Y.; Liu, J.; Kemmer, K. M. *Science* **1997**, *276*, 923. (b) Mercier, L.; Pinnavaia, T. J. *Adv. Mater.* **1997**, *9*, 500. (c) Brown, J.; Richer, R.; Mercier, L. *Microporous Mesoporous Mater.* **2000**, *37*, 41.

(19) (a) Bibby, A.; Mercier, L. *Chem. Mater.* **2002**, *14*, 1591. (b) Walcarius, A.; Etienne, M.; Lebeau, B. *Chem. Mater.* **2003**, *15*, 2161. (c) Walcarius, A.; Delacte, C. *Chem. Mater.* **2003**, *15*, 4181.

(20) (a) Chen, C.-C.; McKimmy, E. J.; Pinnavaia, T. J.; Hayes, K. F. *Environ. Sci. Technol.* **2004**, *38*, 4758. (b) Walcarius, A.; Delacte, C. *Anal. Chim. Acta* **2005**, *547*, 3. (c) Billinge, S. J. L.; McKimmy, E. J.; Shatnawi, M.; Kim, H.-J.; Petkov, V.; Wermeille, D.; Pinnavaia, T. J. *J. Am. Chem. Soc.* **2005**, *127*, 8492.

(21) Tonle, I. K.; Ngameni, E.; Walcarius, A. *Electrochim. Acta* **2004**, *49*, 3435.

This clay sample was converted into its homoionic sodium form[21] denoted Ba−Na^+ hereafter. The well-known MX80 montmorillonite originating from Wyoming (USA), kindly supplied by the Laboratoire Environnement et Minéralurgie (LEM-Nancy, France), was also used for comparison purposes.

Preparation of Porous Clay Heterostructures. The Ba−Na^+ sample was first expanded by reaction with CTAB in a 2-fold excess amount regarding the cation exchange capacity of the clay, at 50 °C for 24 h. After centrifugation, the solid phase denoted Ba−O^+ was recovered and washed successively with ethanol and water to remove the excess of surfactant and air-dried overnight. It was then treated with an excess of DDA (typically 5.0 g DDA in 2 mL ethanol containing 1.0 g Ba−O^+) at 50 °C for 30 min. Thiol-functionalized PCHs were prepared by self-assembly co-condensation of MPTMS and TEOS in the clay galleries, according to a procedure adapted from previous reports,[18] involving typically the addition of a mixture of MPTMS and TEOS to the Ba−O^+/DDA suspension to reach a (MPTMS + TEOS)/DDA molar ration of 7.5 and allowing the mixture to stir at 35 °C for 12 h. Various amounts of MPTMS relative to total precursor quantities (MPTMS + TEOS) were introduced in the synthesis medium to get hybrid materials with various functionalization levels, which have been named hereafter as PCH-SHn% (with n = molar percent of MPTMS ratio in the synthesis medium, ranging from 0 to 35%). The as-synthesized samples were recovered by centrifugation and air-dried for 72 h. Surfactant was extracted using refluxing HCl/ethanol (1 g of solid in a solution containing 3 mL of concentrated HCl and 150 mL of ethanol). The solids were recovered by filtration, washed two times with the ethanol, and air-dried at 70 °C under reduced pressure, and the amount of the thiol group determined from elemental analysis was expressed in millimoles per gram of material.

Apparatus. The structure of clay and PCH-SHn% samples was analyzed by powder X-ray diffraction (XRD) using a classical powder diffractometer (X'PERT PRO/Philips) equipped with a Cu anode (quartz monochromator, $K\alpha_1$ radiation, $\lambda = 1.54056$ Å), and data were collected at room temperature. Their porosity was characterized by nitrogen adsorption−desorption isotherms recorded at 77 K with a coulter instrument (model SA 3100), in the relative pressure range from 10^{-5} to 0.99. Prior to each measurement, the samples were outgassed at 105 °C for a minimum of 16 h under vacuum. Nuclear magnetic resonance spectroscopy with magic angle spinning (MAS NMR) was used to evaluate the effectiveness of organo-functional group incorporation and ^{29}Si and ^{13}C MAS NMR spectra were recorded on a Bruker MSL300 spectrometer. ^{29}Si MAS with proton decoupling experiments were run with a pulse of 1.7 μs ($\pi/6$) and a recycling delay of 80 s. Transmission electron microscopy (TEM) pictures were obtained from a Philips CM20 microscope operating at 200 keV. Particle size distribution was measured using a light scattering analyzer (model LA 920, Horiba), based on the Mie scattering theory.

Sorption Experiments. Batch experiments were performed to determine the capacity of the adsorbents for mercury(II). This was achieved by quantitative analysis of residual mercury(II) concentrations after 24 h reaction under stirring of typically 10 mg/100 mL PCH-SHn% suspensions containing initially a two-times excess amount of the analyte with respect to the thiol content. All solutions were prepared from $Hg(NO_3)_2$ (typically at 0.1 mM). The amount of adsorbed species was calculated by difference with respect to the starting concentrations and expressed per mass of adsorbent by taking into account the solid-to-solution ratio. Quantitative analysis of mercury(II) in solution was carried out by anodic stripping differential pulse voltammetry on a rotating gold electrode,[22] using a μ-autolab potentiostat associated to a GPES electrochemical analysis system (Eco Chemie). Measurements were made in a conventional three-electrode cell containing gold as the working electrode, a Pt wire counter electrode, and an Ag/AgCl reference electrode (Metrohn, 6.0733.100). The electrolytic medium was obtained by dissolving 4.212 g of NaCl (Prolabo), 4.47 g of $EDTANa_2$ (ethylene diamine tetraacetate disodium salt, 99%, from Prolabo), and 120 mL of 70% $HClO_4$ (Riedel-de-Haën) in distilled water to obtain 1 L of solution. Stripping voltammograms were recorded after 30 s of electrolysis at +0.3 V, by scanning potential in the differential pulse mode up to +1.0 V. The analysis was performed after appropriate dilution (if necessary) to fall into the linear range of the technique (0.1−1 μM).

Kinetic Measurements. The speed of mercury(II) binding to PCH-SHn% materials was measured by in situ monitoring of the analyte consumption from suspensions containing the adsorbent particles under constant stirring, which was achieved using a recently developed method based on hydrodynamic voltammetry.[23] A constant reductive potential of −0.5 V is applied to a glassy carbon rotating disk electrode (2000 rd min^{-1}) until reaching a steady state current in 30 mL electrolytic solution (0.1 M $NaNO_3$ at desirable pH) containing Hg(II) at the selected starting concentration. A 20 mg portion of PCH-SHn% is then added into the cell, after being previously dispersed in a 5 mL aliquot of the electrolytic solution under sonication, and mercury consumption is measured as a function of time by recording the decrease of reduction currents at the rotating disk electrode. At the end of the experiment, one part of the cell suspension is filtrated to determine accurately the residual mercury(II) concentration in solution while the other part is analyzed by using a laser granulometer in order to determine the particle size distribution. From the above measurements, it is possible to estimate the apparent diffusion coefficient of the reactive species within the material. This is done by plotting the kinetic data in the form of variation of the Q/Q_0 ratio with time, where Q is the amount of reactant that has reached the binding sites within/on the solid particles at time t, and Q_0 is the maximum amount of accessible binding sites (as experimentally determined from batch sorption capacity measurements), and by fitting the resulting curves to a suitable non-steady-state diffusion model.[19b,c]

Electrochemical Procedures for Permeation Studies. Thin films of PCH-SHn% were deposited onto the surface of solid electrodes to study their permeation properties. To this end, PCH-SHn% suspensions have been prepared by stirring 20 mg of solid particles in 10 mL distilled water for 15 min, which was followed by 1 h sonication, and film deposition was realized by dropping 5 μL of the colloidal clay suspension onto the surface of a glassy carbon electrode (3 mm in diameter). Permeability measurements were carried by hydrodynamic voltammetry using the film-modified rotating disk electrodes in a solution containing the redox probe $[Fe(CN)_6]^{3-}$ (>98%, Fluka) at a

(22) Bonfil, Y.; Brand, M.; Kirowa-Eisner, E. *Anal. Chim. Acta* **2000**, *424*, 65.
(23) (a) Gueshi, T.; Tokuda, K.; Matsuda, H. *J. Electroanal. Chem.* **1979**, *101*, 29. (b) Gough, D. A.; Leypoldt, J. K. *Anal. Chem.* **1979**, *51*, 439. (c) Peerce, P. J.; Bard, A. J. *J. Electroanal. Chem.* **1980**, *114*, 89. (d) Ikeda, T.; Schmehl, R.; Denisevich, P.; William, K.; Murray, R. W. *J. Am. Chem. Soc.* **1982**, *104*, 2683. (e) Leddy, J.; Bard, A. J. *J. Electroanal. Chem.* **1983**, *153*, 223.
(24) (a) Tonle, I. K.; Ngameni, E.; Njopwouo, D.; Carteret, C.; Walcarius, A. *Phys. Chem. Chem. Phys.* **2003**, *5*, 4951. (b) Tonle, I. K.; Ngameni, E.; Tcheumi, H. L.; Tchieda, V.; Carteret, C.; Walcarius, A. *Talanta* **2008**, *74*, 489.

concentration of 1 mM (+0.1 M KCl as supporting electrolyte). Rotation rates were varied in the 50−5000 rpm range.

3. Results and Discussions

3.1. Preparation and Physicochemical Characterization of PCH-SH*n*%. The pristine clay sample used here is the fine fraction of natural smectite of structural formula $Ca_{0.06}K_{0.38}Na_{0.45}(Si_{7.02}Al_{0.98})(Al_{3.67}Fe_{0.17}Mg_{0.13}Ti_{0.06})O_{20}(OH)_4$, originating from the Baba deposit in Cameroon, which has been first purified and then transformed into its sodium homoionic form (Ba−Na^+); its full characterization has been reported earlier.[24] Ba−Na^+ was expanded by ion exchange with cetyltrimethylammonium cations (to form Ba−O^+) according to a previously described procedure,[11,13] and spreading of clay sheets was pointed out by XRD (Figure 1) through the shift of the 001 reflection peak to lower 2θ angles (i.e., from 2θ = 8.62 (Ba−Na^+) to 2θ = 4.05 (Ba−O^+), corresponding to *d* spacings of 10 and 22 Å, respectively). Passing from Ba−Na^+ to Ba−O^+ also resulted in a significant lack of porosity of the material (Table 1). Cosurfactant, dodecylamine (DDA), was then intercalated in the interlayer regions of Ba−O^+, and precursors (TEOS and MPTMS) were added to the suspension to form the organosilica network. Hydrolysis and self-assembly co-condensation of the precursors is expected to be confined to the gallery regions of the clay as they exclusively contain water molecules and the structure-directing surfactant.[8,10,18]

The XRD patterns of surfactant-extracted PCH-SH*n*% samples shown in Figure 2 reveal a peak at low 2θ values, which can be assigned to the d_{001} reflection, indicating a structural order at the mesoporous level. No multiple reflections can been seen, consistent with previous reports on similar heterostructures,[11,13b] but contrary to what was sometimes observed for other PCHs.[15,18a] All PCH-SH*n*% materials were characterized by 001 reflections corresponding to basal spacing from 27 to 40 Å, indicating gallery expansion as a result of (organo)silica network formation. Both of these values and the intensity of XRD lines were found to decrease when increasing the amount of organo-functional groups in the solid, suggesting that the framework mesostructures were better expressed at low organic group content. Note that template removal by solvent extraction induced some lattice contraction, as evidenced by some decrease in d_{001} values (e.g., from 39 to 30 Å for PCH-SH10%). The same PCH synthesis procedure was also applied to the well-known MX80 clay sample and gave rise to similar observations, with gallery heights yet lower with MX80 samples than for "Ba" ones (e.g., d_{001} values equal to 36 and 32 Å for PCH-SH5%, respectively, from Ba and MX80, as calculated from XRD measurements on surfactant-extracted samples). High resolution TEM was further applied to point out the clay-to-PCH transformation (Figure 3). Comparing parts A and B on this figure enables the observation of significant increase in the gallery height when passing from Ba−Na^+ to PCH-SH5% (intragallery space appearing in lighter contrast between the dark clay layers). One can even notice (especially in the center of Figure 3B) some white "points" between the clay sheets, which could correspond to intercalated mesochannels formed upon self-assembly co-condensation of precursors in the presence of surfactant template. This observation, which was also made by another group on saponite-based PCHs,[11b] along with the fact that TEM pictures did not feature any phase separation (energy-dispersive X-ray analysis performed on various distinct portions of samples always revealed the presence of Al; i.e., no detectable pure silica phases), contributes to support the preferential (if not exclusive) formation of mesoporous (organo)silica networks in close association to the clay sheets and not as distinct particles, in agreement with previous works on related heterostructures.[8,10−15,18] Of course, one cannot state unambiguously that no hexagonal silica mesophase has been formed outside the clay particles, but this contribution (if existing) is expected to be small on the basis of the above observations as well as from the fact that the

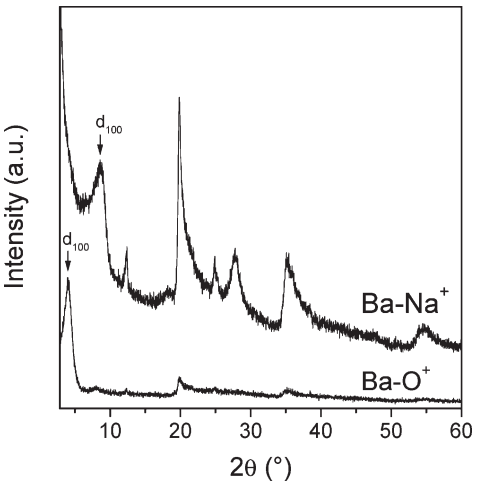

Figure 1. Powder XRD patterns of the homoionic sodium form of the natural "Ba" clay sample (Ba−Na^+) and that of the same sample treated with cetyltrimethylammonium (Ba−O^+).

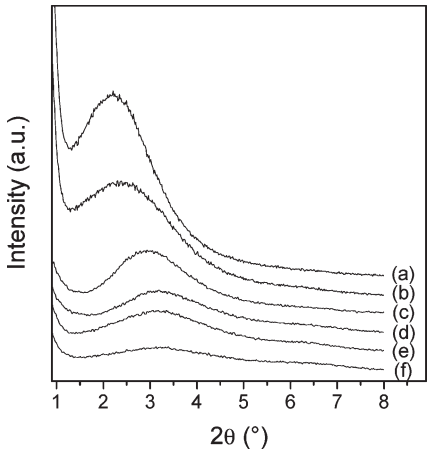

Figure 2. Powder XRD patterns of surfactant-extracted thiol-functionalized porous clay heterostructures (PCH-SH*n*%, where *n* represents the molar percent of MPTMS in the synthesis medium): (a) PCH; (b) PCH-SH5%; (c) PCH-SH10%; (d) PCH-15%; (e) PCH-SH25%; and (f) PCH-SH35%.

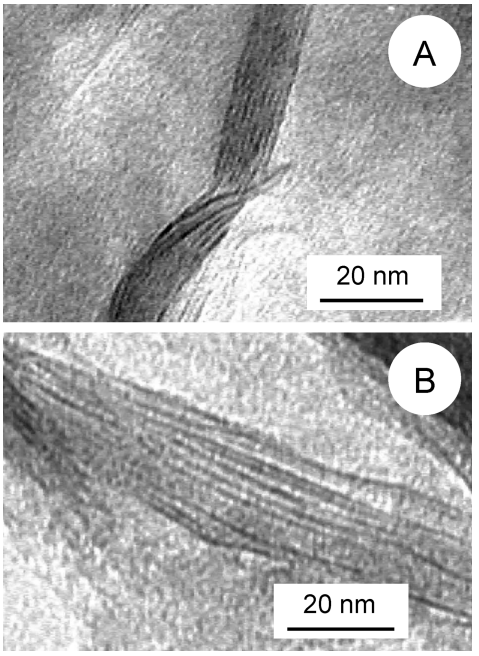

Figure 3. TEM micrographs of the homoionic sodium form of the natural Ba clay sample, Ba−Na^+ (A) and solvent-extracted PCH-SH5% (B).

surfactant-extracted Ba−O^+ sample (i.e., not transformed into PCH) was no more expanded whereas the clay layers in PCH remained expanded after template removal due to the presence of silica between the clay sheets.

The templated structure of PCH-SH*n*% materials was also denoted from nitrogen adsorption−desorption isotherms (Figure 4). Part A of the figure compares the curves obtained for the starting Ba−Na^+ sample, that treated with the surfactant template (Ba−O^+), and that corresponding to the nonfunctionalized PCH sample. The results clearly indicate that the transformation of Ba−Na^+ into Ba−O^+ resulted in dramatic decrease in porosity because the bulky surfactant species occupies the whole intragallery space. Data obtained from both energy-dispersive analysis of X-rays (1.32% Na and no N in Ba−Na^+; no Na and 6.51% N in Ba−O^+) and X-ray photoelectron spectroscopy (disappearance of Na_{1s} with concomitant growth of the N_{1s} and C_{1s} signals in Ba−O^+) demonstrate successful exchange of Na^+ by CTA^+ and incorporation of DDA. After formation of PCH and subsequent surfactant extraction (whose effectiveness was checked by IR spectroscopy), the resulting isotherm is a typical "knee curve", which is characteristic of supermicropores around 20−30 Å.[25] Actually, all PCH-SH*n*% were highly porous (Figure 4B), with specific surface areas higher by about 1 order of magnitude in comparison to the pristine clay and much higher pore volumes as well (Table 1). By adding organosilane, the flat part disappeared, the shape of the isotherm became characteristic of microporous materials (V_{micro}/V_{tot} in the 50−60% range), and pore sizes were found to decrease upon functionalization (see Figure A in the Supporting Information). These values are lower than pore diameters usually reported for CTAB-templated thiol-functionalized mesoporous materials obtained by the one-step co-condensation route (20−30 Å),[19c,26] suggesting again that silica channels described here are primarily formed between the clay sheets and not mainly as pure phase wormhole-motif mesostructures. The step in desorption observed at $p/p_0 = 0.47$ is characteristic of the presence of additional macropores existing between clay sheets and connected to the exterior by the porosity of the PCH. The pore volume of these materials have thus been taken at the end of the filling of the micropores (at around $p/p_0 = 0.3$), and these values have been added in Table 1. They indicate that the textural parameters of functionalized materials were found to decrease as a result of increasing amounts of organic groups in the mesopore channels, but porosity losses were rather limited up to 15% SH. Even the highly functionalized solids exhibited specific surfaces areas more than 5 times larger than the pristine clay (Table 1).

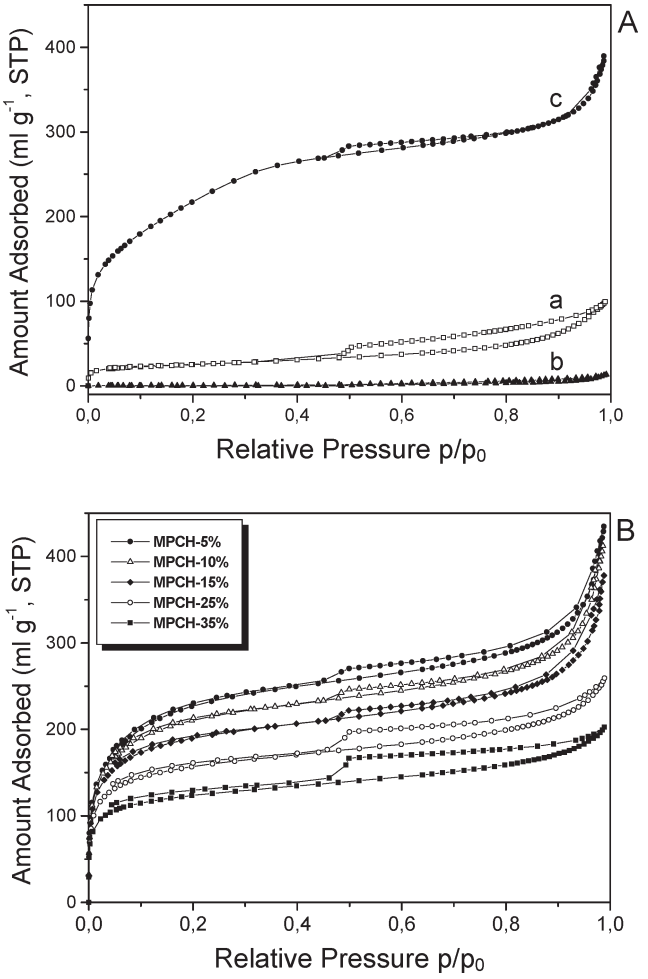

Figure 4. Nitrogen adsorption/desorption isotherms of various clay and PCH samples: (A) the starting Ba−Na^+ clay sample (a), the same sample treated with cetyltrimethylammonium Ba−O^+ (b), the nonfunctionalized PCH sample (c); (B) the thiol-functionalized PCH-SH*n*% (with *n* equal to 5, 10, 15, 25, and 35).

(25) Greg, S. J.; Sing, K. S. W. *Adsorption, Surface Area and Porosity*, 2nd ed.; Academic Press Inc.: San Diego, 1982.

(26) Gaslain, F.; Delacôte, C.; Lebeau, B.; Walcarius, A. *J. Sol−Gel Sci. Technol.* **2009**, *49*, 112.

Table 1. Some Physicochemical Data of the Pristine "Ba" Clay Sample, its Homoionic Sodium Form (Ba−Na$^+$), the Same Sample Treated with Cetyltrimethylammonium (Ba−O$^+$), the Nonfunctionalized Porous Clay Heterostructure (PCH), and Various Thiol-Functionalized Porous Clay Heterostructures (PCH-SH*n*%, with *n* Varying between 5 and 35, Corresponding to the Molar Percent Amount of MPTMS Relative to the Total Amount of Silane Precursors in the Synthesis Medium)[a]

	nitrogen adsorption−desorption					
sample	surface area/m^2 g^{-1}	total pore volume/cm^3 g^{-1}	micropore volume/cm^3 g^{-1}	pore volume at p/p_0 = 3/cm^3 g^{-1}	XRD d_{100}/Å	amount of thiol groups/mmol g^{-1}
Ba (raw clay)	79	0.13			10	
Ba−Na$^+$	81	0.14			10	
Ba−O$^+$	2	0.02			22	
PCH	773	0.56	0.36	0.37	40	
PCH-SH5%	816	0.59	0.32	0.37	36	0.7
PCH-SH10%	723	0.55	0.33	0.33	30	1.1
PCH-SH15%	667	0.54	0.26	0.30	27	1.5
PCH-SH25%	577	0.42	0.23	0.27	27	2.2
PCH-SH35%	401	0.27	0.15	0.18	27	2.9

[a] All data have been obtained after template extraction.

Formation of the (organo)silica network in PCH-SH*n*% materials was confirmed by ^{29}Si NMR. Typical results are illustrated in Figure 5. For the nonfunctionalized PCH (denoted PCH or PCH-SH0%), distinct resonances are observed for the siloxane [Q^n = Si—(OSi)$_n$—(OH)$_{4-n}$, n = 2−4; Q^4 at −110 ppm, Q^3 at −101 ppm, and Q^2 at −91 ppm], with a great majority of highly connected centers ($Q^4 > Q^3 \gg Q^2$; see part A of the figure), the intrinsic Q resonance for the clay sheet being most probably hidden in these signals as no distinct peak can be seen (it should appear somewhere between Q^2 and Q^3,[18a] but its contribution is expected to be low as the acid treatment applied to template removal contributed to hydrolyze a great part of Al centers in the materials). In addition to these siloxane centers, organosiloxane [T^m = RSi—(OSi)$_m$—(OH)$_{3-m}$, m = 1−3; T^3 at −65 ppm, T^2 at −56 ppm] species appear in the spectra (see parts B and C of the figure, respectively, for PCH-SH10% and PCH-SH25%) indicating successful incorporation of organosilicon into the hybrid structures. The amount of organo-functional groups linked to the structure was found to increase proportionally to the MPTMS:TEOS ratio in the synthesis medium. Q^4, Q^3, and T^3 species are the main components for all materials, which demonstrates that the silica network is well condensed. The relative amounts of Q^n units for the highly functionalized materials indicate, however, a lower degree of condensation (higher Q^2 and lower Q^4 content values) in comparison with the solids containing less mercaptopropyl groups. The presence of sulfur-containing moieties was also demonstrated by elemental analysis, and materials containing up to 2.9 mmol of thiol groups per gram of mesoporous solid have been obtained (Table 1). Up to 15% MPTMS in the synthesis medium, all mercaptopropyl groups were readily incorporated in the final material whereas less-than-complete MPTMS co-condensation was observed at higher contents. Also, solid state ^{13}C NMR data indicate the presence of some residual ethoxy groups (characteristic signals at 16.9 and 59.9 ppm) due to incomplete hydrolysis of some silane or organosilane precursors.

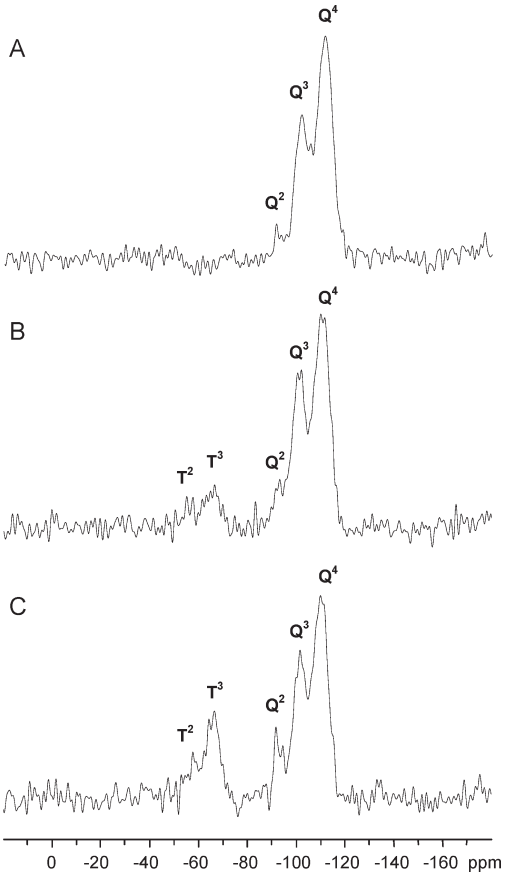

Figure 5. ^{29}Si MAS NMR spectra of surfactant-extracted porous clay heterostructures: PCH (A), PCH-SH10% (B), and PCH-SH25% (C), in the shift range from 20 to −180 ppm.

3.2. Mercury(II) Binding to PCH-SH*n*%. Accessibility to active centers in PCH-SH*n*% materials was characterized by using Hg(II) as a probe because this analyte is known to

form complexes with thiol groups immobilized on silica surfaces.[17,19,20] More interestingly, varying pH is likely to induce the formation of either charged complexes (−S−Hg^+ at pH values lower than 3; see eq 1) or neutral species (−S−HgOH at pH higher than 3; see eq 2),[20b] some other mercury-thiolate forms with variable coordination environments being also reported[20a,c] from experiments performed around pH 3 where both Hg^{2+}, $HgOH^+$, and $Hg(OH)_2$ species are expected to coexist in solution.[27]

$$\equiv Si{-}C_3H_6{-}SH + Hg^{2+}, 2NO_3^- \rightarrow Si{-}C_3H_6{-}S{-}Hg^+, NO_3^- + HNO_3 \quad (1)$$

$$\equiv Si{-}C_3H_6{-}SH + HgOH^+, NO_3^- \rightarrow Si{-}C_3H_6{-}S{-}HgOH + HNO_3 \quad (2a)$$

$$\equiv Si{-}C_3H_6{-}SH + Hg(OH)_2 \rightarrow Si{-}C_3H_6{-}S{-}HgOH + H_2O \quad (2b)$$

Figure 6 shows the variation of the amount of bonded Hg(II) to PCH-SH*n*% materials as a function of their functionalization level. Data have been recorded at two distinct pH values (2 and 4) where Hg(II) species are mainly in the form of Hg^{2+} (pH 2) or $Hg(OH)_2$ (pH 4). The $HgOH^+$ form is negligible (< 3%) at these two pH values.[27] Independent of the adsorbent type, Hg(II) uptake was always superior at pH 4 (compare curves a and b in Figure 6). This is explained by the fact that $Hg(OH)_2$ is likely to be immobilized not only via complexation with thiol groups but also through reaction with residual acidic silanol groups on the silica surface (eq 3).[28] Hg(II) adsorption on silica has been thoroughly studied, and the chemisorbed surface complex (≡Si—O—HgOH) well identified.[29] This is also the reason why Hg(II) uptake, yet small (0.2 mmol g^{-1}), was observed at pH 4 on the nonfunctionalized PCH sample (i.e., PCH-SH0%).

$$\equiv Si{-}OH + Hg(OH)_2 \rightarrow Si{-}O{-}HgOH + H_2O \quad (3)$$

Another explanation for such a difference is related to the fact that a charged complex is formed at pH 2 (eq 1), inducing thereby electrostatic repulsion for further ingress of Hg^{2+} inside the mesochannels, which was reported to be more dramatic for highly functionalized materials.[20b] Actually, 100% accessibility (i.e., each thiol group complexing one mercury ion) was observed at pH 2 for adsorbents made from MPTMS contents up to 15%, consistent with what was reported for correspondingly functionalized mesoporous silica particles.[17,19c] This arises from the well-ordered structure of PCH-SH*n*%, imparting easy access to the functional groups. Some restricted access was however observed in highly functionalized PCH-SH*n*% (e.g., about 80% in PCH-SH35%) as a consequence of the aforementioned electrostatic shielding effect in a closer environment (pore volumes are significantly lower in PCH-SH25% and PCH-SH35% relative to other PCH-SH*n*% materials; see Table 1). Such restriction did not occur at pH 4 where a neutral ≡Si—O—HgOH complex was formed, generating uptake capacities directly proportional to the amount of thiol groups in the material, and even slightly superior due to reaction of $Hg(OH)_2$ with surface hydroxyl groups (eq 3). Modifying the intragallery regions of clays by self-assembly co-condensation of TEOS and MPTMS thus provides an elegant way to increase the clay capacity toward heavy metal adsorption. The maximum Hg(II) loading capacity evaluated here at about 3.1 mmol g^{-1}, at pH 4, for PCH-SH35% constitutes the highest uptake level ever report on modified clay sorbents. By comparison, the highest capacity attained with the same Ba clay sample grafted with MPTMS was less than 1 mmol g^{-1},[24a] and even much lower values have been reported for mercaptopropyl-grafted montmorillonite (0.33 mmol g^{-1}),[6b] for which calculated accessibilities were respectively equal to 36% and 10% with respect to the amount of thiol groups in the materials. Even more remarkable is the 100% accessibility achieved here with PCH-SH*n*% materials obtained by the one-step co-condensation method in comparison to lower performance achieved with PCH postgrafted with mercaptopropyl groups for which 67% accessibility has been reported (for a material containing 1.1 mmol g^{-1} SH group).[15] Table 2 provides comparison data for mercury uptake by a wide range of thiol-functionalized mesoporous silica (HMS,

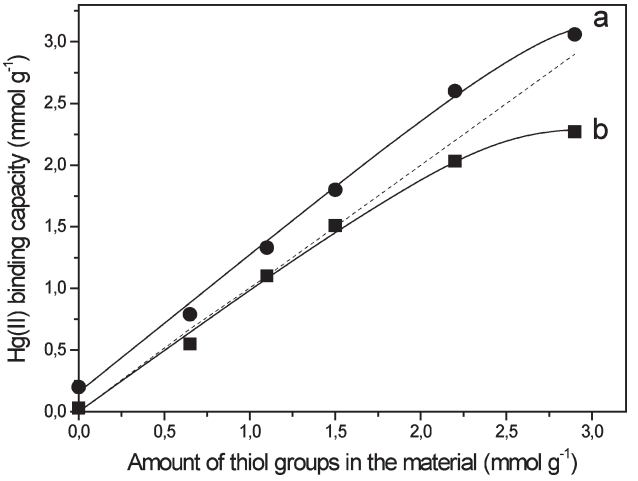

Figure 6. Variation of the amount of adsorbed mercury(II) onto PCH-SH*n*% samples, as a function of the thiol group content in the material (from elemental analysis), as measured at two pH values: pH 4 (a) and pH 2 (b). The starting mercury(II) concentrations in the PCH-SH*n*% suspension were adjusted to reach an amount of Hg(II) species twice as much as the thiol content. The dashed line represents quantitative Hg(II) uptake relative to SH.

(27) Baes, C. F., Jr.; Mesner, R. E. *The hydrolysis of cations*; Wiley: New York, 1976; p 311.
(28) (a) Walcarius, A.; Devoy, J.; Bessière, J. *Environ. Sci. Technol.* **1999**, *33*, 4278. (b) Walcarius, A.; Bessière, J. *Chem. Mater.* **1999**, *11*, 3009.
(29) (a) Tiffreau, C.; Lützenkirchen, J.; Behra, P. *J. Colloid Interface Sci.* **1995**, *172*, 82. (b) Bonnissel-Gissinger, P.; Alnot, M.; Lickes, J.-P.; Ehrhardt, J.-J.; Behra, P. *J. Colloid Interface Sci.* **1999**, *215*, 313.
(30) (a) Liu, J.; Feng, X.; Fryxell, G. E.; Wang, L.-Q.; Kim, A. Y.; Gong, M. *Adv. Mater.* **1998**, *10*, 161. (b) Mattigod, S. V.; Feng, X.; Fryxell, G. E.; Liu, J.; Gong, M. *Sep. Sci. Technol.* **1999**, *34*, 2329. (c) Chen, X.; Feng, X.; Liu, J.; Fryxell, G. E.; Gong, M. *Sep. Sci. Technol.* **1999**, *34*, 1121.
(31) (a) Brown, J.; Mercier, L.; Pinnavaia, T. J. *Chem. Commun.* **1999**, 69. (b) Mercier, L. *Stud. Surf. Sci. Catal.* **2000**, *129*, 739. (c) Mercier, L.; Pinnavaia, T. J. *Environ. Sci. Technol.* **1998**, *32*, 2749.
(32) Lee, B.; Kim, Y.; Lee, H.; Yi, J. *Microporous Mesoporous Mater.* **2001**, *50*, 77.

Table 2. Comparison Data for Hg(II) Binding to Thiol-Functionalized Mesoporous Silica[a]

mesoporous material type	functionalization method	thiol group content (mmol g^{-1})	$Hg^{(II)}$ ads capacity (equil time; pH) (mmol g^{-1})	Hg(II) diff coef range (cm^2 s^{-1})	refs
FMMS	SAMMS	5.2	2.5 (2 h; pH 3, 7, 9)		17a and 30a
FMMS	SAMMS	2.8	1.35 (4 h; pH 3, 5, 7, 9)		30b
FMMS	SAMMS		3.1		30c
HMS	grafting	1.5	1.5 (18 h)		17b
HMS	co-cond	0.35−1.3	0.19−0.65 (24 h)		31a
HMS	co-cond	0.85	0.7 (24 h)		31b
HMS	co-cond	2.38	1.51 (10 h; pH 4)		32
HMS	co-cond	0.8−2.3	0.24−1.26 (24 h)		33
HMS and MCM-41	grafting	0.57−1.5	0.55−1.5 (18 h)		31c
MCM-41	grafting	1.0−2.8	0.8−1.4 (pH 2)	10^{-11}−10^{-10}	19b and 34a
MCM-41 (and HMS)	co-cond	0.53−7.0	0.5−3.8 (24 h; pH 2)	$5-50 \times 10^{-11}$	19c
MCM-41 (and HMS)	co-cond	1.55−4.0	1.0−2.5 (24 h; pH 2) 1.5−3.5 (24 h; pH 4)		20b
MCM-48	grafting	2.7	1.4 (pH 2)	10^{-11}−10^{-10}	19b and 34a
MSU	co-cond	0.47−2.3	up to 2.3 (24 h)		17c
MSU	co-cond	0.5−1.49	0.52−1.49 (24 h)	10^{-11}−10^{-10}	19a
PMO	co-cond	6.5−7.7	2.2−2.5 (12 h)		35
SBA-15	grafting	1.0	1.0 (pH 2)	10^{-9} range	19b
SBA-15	co-cond	0.54−2.9	0.55−2.88 (24 h; pH 0−7)		36a
SBA-15	co-cond	0.5−4.1	0.5−4.1		36b
SBA-15	grafting		0.26 (pH 2)−0.27 (pH 4)	8×10^{-8}	34b
	co-cond		1.15 (pH 2 and 4)	1×10^{-8}	
SBA-16	grafting		0.38 (pH 2)−0.42 (pH 4)	5×10^{-9}	34b
	co-cond		1.29 (pH 2)−1.37 (pH 4)	2×10^{-9}	
PCH	grafting	1.1	0.74 (18 h)		15
PCH	co-cond	0.7−2.9	0.5−2.3 (pH 2) 0.7−3.1 (pH 4)	10^{-11}−10^{-10}	this work

[a] Abbreviations: FMMS functionalized monolayer on ordered mesoporous silica; HSM hexagonal mesoporous silica; MCM: Mobil Composition of Matter; MSU: Michigan State University; PMO: Periodic Mesoporous Organosilica; SBA: Santa Barbara Amorphous; PCH: Porous Clay Heterostructure; SAMMS: Self-Assembled Monolayer on Mesoporous Silica.

MCM, MSU, SBA, ...),[17,19,30−36] showing that capacities measured here for PCH-SH*n*% materials are among the highest values.

The speed at which a reactant is likely to reach the active centers located inside a highly porous material is of critical importance for various applications including catalysis, separation sciences, drug delivery systems or electrochemistry.[37] This has been investigated here by studying the rate of Hg(II) uptake by PCH-SH*n*% materials and discussing the associated kinetics with respect to the degree of functionalization and therefore the level of ordering of the adsorbents. This was performed using an electrochemical method based on hydrodynamic voltammetry, which was previously developed by our group to monitor mass transport processes in mesoporous silica,[19b,c] consisting in the in situ semicontinuous monitoring of Hg(II) consumption as a function of time from aqueous suspensions of PCH-SH*n*% particles. Representative results are depicted in Figure 7 showing dramatic variations in the speed of Hg(II) uptake as a function of pH (compare parts A and B) and on the type of PCH-SH*n*% material (compare curves a−f in the figures). The results are presented in the form of Q/Q_0 versus time plots where Q represents the amount of bound Hg(II) at time t and Q_0 is the maximum amount of accessible binding sites for the target analyte species (i.e., the amount of sorbed Hg^{II} after 24 h). Data indicate a strong influence of the functionalization degree on the rate of Hg(II) binding and this effect was significantly different at pH values of 2 and 4. Sorption kinetics, which might be useful to engineers who would use these materials, can be derived from these data and the results have been reported for Hg(II) adsorption at both pH 2 and 4 in the Supporting Information (see Figure B). They indicate rather high values (~10 mmol g^{-1} min^{-1}) at the beginning of the experiments and then lower rates as far as the amount of remaining free sites decreased. Again, the functionalization level and degree of structural organization were found to affect these values in an antagonist way: enhanced sorption kinetics as a result of increased thiol group contents and restricted filling rates when mass transport became slower. For example, at pH 4, the values measured at 33% filling ($Q/Q_0 = 0.33$) were equal to 0.15, 0.34, 0.38, 0.25, and 0.07 mmol g^{-1} min^{-1}, respectively, for PCH-SH5%, 10%, 15%, 25%, and 35% (i.e., maximal for PCH-SH15%). This trend was even more marked at pH 2.

More accurate description and interpretation of Q/Q_0 versus time curves can be made on the basis of the apparent diffusion coefficients that can be evaluated from fitting these curves by taking into account the size of

(33) Nooney, R. I.; Kalyanaraman, M.; Kennedy, G.; Maginn, E. J. *Langmuir* **2001**, *17*, 528.
(34) (a) Gaslain, F.; Delacote, C.; Lebeau, B.; Marichal, C.; Patarin, J.; Walcarius, A. *Stud. Surf. Sci. Catal.* **2007**, *165*, 417. (b) Lesaint, C.; Frebault, F.; Delacote, C.; Lebeau, B.; Marichal, C.; Walcarius, A.; Patarin, J. *Stud. Surf. Sci. Catal.* **2005**, *156*, 925.
(35) Alauzun, J.; Mehdi, A.; Reye, C.; Corriu, R. J. P. *Chem. Commun.* **2006**, 347.
(36) (a) Aguado, J.; Arsuaga, J. M.; Arencibia, A. *Ind. Eng. Chem. Res.* **2005**, *44*, 3665. (b) Aguado, J.; Arsuaga, J. M.; Arencibia, A. *Microporous Mesoporous Mater.* **2008**, *109*, 513.
(37) (a) Walcarius, A. *C. R. Chim.* **2005**, *8*, 693. (b) Clark, J. H.; MacQuarrie, D. J.; Tavener, S. J. *Dalton Trans.* **2006**, 4297. (c) Gu, J.; Fan, W.; Shimojima, A.; Okubo, T. *Small* **2007**, *3*, 1740. (d) Slowing, I. I.; Trewyn, B. G.; Giri, S.; Lin, V. S. *Adv. Funct. Mater.* **2007**, *17*, 1225. (e) Amatore, C.; Oleinick, A.; Klymenko, O. V.; Delacote, C.; Walcarius, A.; Svir, I. *Anal. Chem.* **2008**, *80*, 3229.

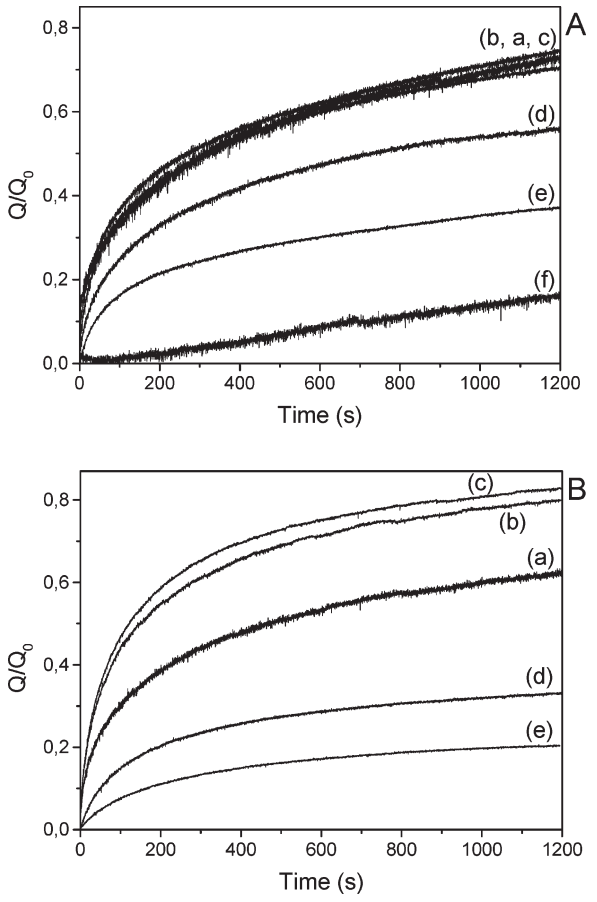

Figure 7. Uptake of mercury(II) as a function of time, at pH 4 (A) or pH 2 (B), using various PCH adsorbents: (a) PCH-SH5%, (b) PCH-SH10%, (c) PCH-SH15%, (d) PCH-SH25%, (e) PCH-SH35%, and (f) PCH-SH0% (i.e., PCH). Experiments have been performed from suspensions containing 20 mg of adsorbent particles in 35 mL solution containing Hg(II) at a starting concentration corresponding to 105% of the maximal binding capacity of each of the material, as determined from data of Figure 6.

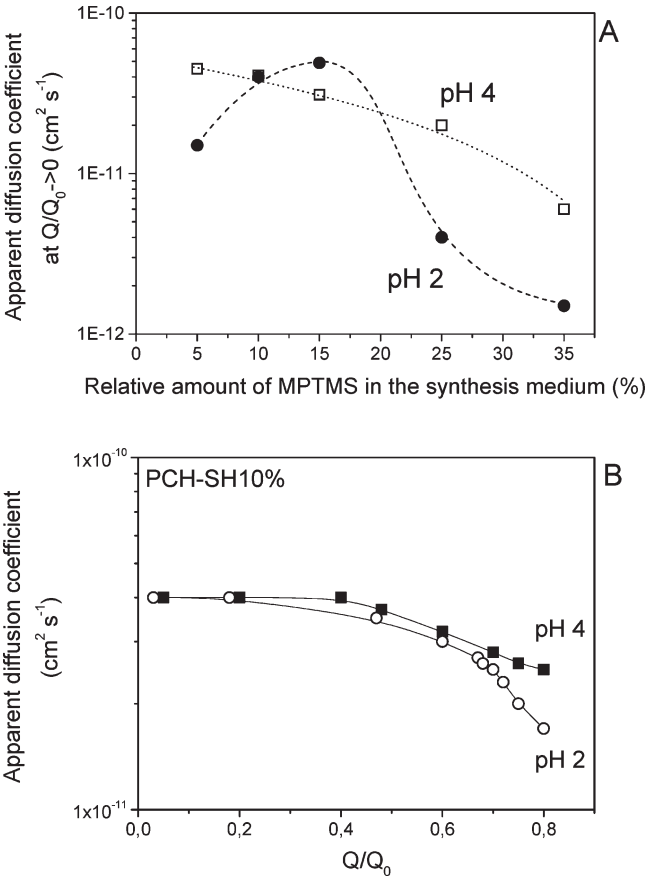

Figure 8. (A) Variation of the apparent diffusion coefficients for Hg(II) in PCH-SHn%, as measured at the beginning of sorption experiments [$\lim_{t=0}(Q/Q_0 = f(t))$] at pH 2 or pH 4, expressed as a function of the functionalization level (relative to the amount of MPTMS in the synthesis medium). (B) Variation of the apparent diffusion coefficients for Hg(II) in PCH-SH10%, as measured at pH 2 or pH 4, expressed as a function of the Hg(II) filling level (Q/Q_0).

PCH-SHn% particles in the suspension. Figure 8A compares these values calculated using eq 4, which is valid to get diffusion coefficients corresponding to the early times of the sorption experiments in conditions of spherical diffusion[38] (which is quite acceptable for the filling of particles in suspension, at least in first approximation, in order to compare the results obtained with a family of solids of approximately the same size and shape), expressed as a function of the functionalization level of the adsorbent.

$$\lim\left(\frac{\partial\left(\frac{Q}{Q_0}\right)}{\partial(\sqrt{t})}\right)_{t\to 0} = 6\sqrt{\frac{D_{app}}{\pi a^2}} \qquad (4)$$

Where D_{app} is the apparent diffusion coefficient and a is the average particle radius (as determined from particle size distributions measurements).

At pH 4, one can clearly see rather high D_{app} values in the range $2-4 \times 10^{-11}$ cm^2 s^{-1} for Hg(II) in PCH-SH5% to PCH-SH15%, which then decreased more rapidly down to 10^{-11} cm^2 s^{-1} when increasing further the functionalization level. This trend can be explained by the decrease in porosity in the PCH-SHn% series (Table 1) as Hg(II) are intended to diffuse in a more restricted environment when passing from PCH-SH5% to PCH-SH35%. The situation was markedly different at pH 2 for which the decrease in D_{app} values when passing from PCH-SH15% to PCH-SH35% was more abrupt than at pH 4 (e.g., D_{app} down to 1.5×10^{-12} cm^2 s^{-1} in PCH-SH35%) and some diffusional limitations started to be observed for PCH-SH5% (Figure 8A). This behavior is attributed to the formation of a positively charged $-$S$-$Hg$^+$ complex in the porous material, generating thereby some resistance to mass transport of Hg^{2+} species. This restriction was more marked in materials containing higher thiol group contents (because of higher density of organo-functional groups) as well as in the more ordered PCH-SH5% solid due to the enhanced electrostatic shielding effect in mesopore channels of longer dimension (expected to exist in long-range order materials). Such electrostatic repulsion in well-ordered mesostructures occurring when charged moieties are formed onto the walls of mesopore channels has been already reported for mesoporous organosilica materials.[19b,c,20b,37e] This effect can be also evidenced from the variation of D_{app} values as

(38) Crank, J. *The Mathematics of Diffusion*; Clarendon Press: Oxford, 1975.

a function of the filling level of the adsorbent with Hg(II) species. As expected from the place occupied by Hg(II) species, the diffusion rates were found to decrease when progressively filling the material but this decrease was more important at pH 2 than at pH 4, as shown in Figure 8B for the PCH-SH10% sample (chosen for the illustration as this sample was characterized by the same D_{app} values at Q/Q_0 tending to zero, but the same trend was observed for all samples). The above results demonstrate the advantage in using highly porous and mesostructured PCHs to improve mass transfer rates to the active centers, in any cases if the uptake reaction does not generate charged moieties in the ordered material, short-range order being preferred over long-range order in case of charge formation. Table 2 shows that D_{app} values measured in PCH-SH*n*% materials are of the same order of magnitude as those observed for pure silica thiol-functionalized MCM-41 or MCM-48 adsorbents exhibiting approximately the same pore size while slightly higher values have been reported for larger pore SBA-15 and SBA-16 materials. The interest of the PCH series is thus not intrinsically improved performance in terms of enhanced diffusion rates but rather relies on their particular morphology (mesochannels located between clay platelets) making possible and easy their spatial arrangement as stable thin films on solid supports, which is not possible when using conventional mesoporous organosilica powders (which requires the addition of a polymeric binder to get mechanically stable coatings).[18c] An illustrative example of such an attractive feature is provided in the Supporting Information (see Figure C) in the case of Hg(II) electrochemical sensing using a PCH-SH-film electrode.

3.3. Permeability through PCH Films on Electrode. In attempt to point out further the interest in mesostructuring the intragallery regions of clays to impart fast mass transport in these materials, all PCH samples prepared here were deposited as thin films on electrode surfaces and hydrodynamic voltammetry[39] was applied to the resulting clay modified electrodes to get insights in their permeability toward $[Fe(CN)_6]^{3-}$ species chosen as the redox probe. It is known indeed that using a rotating disk electrode at various rotation rates leads to an increase of limiting currents i_l (Figure 9A) that can be related to the permeability of a porous film deposited onto the electrode surface by the following relation (eq 5).[23d]

$$\frac{1}{i_l} = \frac{d}{nFAD_f PC_s} + \frac{1}{0.62nFAD_s^{2/3}\nu^{-1/6}\omega^{1/2}D_s} \qquad (5)$$

where n is the number of exchanged electrons per mole of redox probe, F is the Faraday constant, A is the electrode surface area, D_s is the diffusion coefficient of the probe in solution, ν is the kinematic viscosity, ω is the angular rotation rate of the electrode, C_s is the probe concentration in solution, d is the film thickness, P is the permeation coefficient of the probe into the film, and D_f is the diffusion coefficient of the probe in the film. The permeability is usually described as the product PD_f.

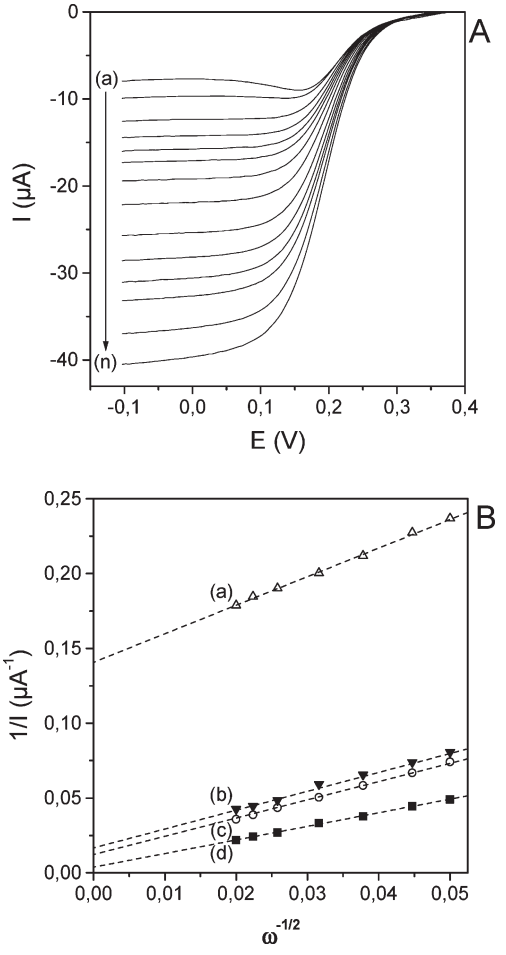

Figure 9. (A) Typical hydrodynamic voltammograms recorded at 20 mV s^{-1} in a solution containing 10^{-3} M $[Fe(CN)_6]^{3-}$ (+0.1 M KCl) at a glassy carbon electrode (GCE) modified with a PCH-SH10% film (curves a−n, electrode rotation rates: 50, 100, 200, 300, 500, 700, 1000, 1400, 2000, 2500, 3000, 4000, and 5000 rpm, respectively). (B) Reciprocal Levich plots obtained from experiments performed as in part A, using GCE modified with $BaNa^+$ (a) PCH-SH35% (b), PCH-SH10% (c), and bare GCE (d).

As shown from this equation, plotting the values $1/i_l$ as a function of $\omega^{-1/2}$ would give rise to a straight line. If $D_s^{2/3}\nu^{-1/6}\omega^{1/2} \ll PD_f/d$ (e.g., absence of film, thin film with large PD_f or extremely thin film), the diffusion through the Levich layer is the slower of the two and the Levich plot is linear with zero intercept (see curve "d" in Figure 9B). If diffusion through the film is slower, the plot of $1/i_l$ versus $\omega^{-1/2}$ is linear and PD_f/d can be evaluated from the intercept. The higher the intercept, the lower the film permeability.

Figure 9B illustrates some typical data obtained with various clay and PCH films deposited by drop-coating on glassy carbon electrodes. They clearly indicate the advantage of PCH, with permeability values for PCH-SH*n* % ($PD_f/d = 0.9-1.4 \times 10^{-2}$ cm s^{-1}) higher by 1 order of magnitude than that of a nonmodified Ba−Na^+ film ($PD_f/d = 1.0 \times 10^{-3}$ cm s^{-1}), demonstrating thereby the interest in generating mesochannels in the clay galleries to improve dramatically the permeation properties of

(39) Bard, A. J.; Faulkner, L. R. *Electrochemical Methods. Fundamental and Applications*, 2nd ed.; John Wiley & Sons Inc.: New York, 2001.

resulting clay films on electrodes. This has been notably exploited to enhance the sensitivity of clay modified electrodes applied in preconcentration electroanalysis.[18c] Data in Figure 9B also feature a small, yet visible, difference between the films pepared from PCH-SH10% ($PD_f/d = 1.4 \times 10^{-2}$ cm s^{-1}) and PCH-SH35% ($PD_f/d = 0.9 \times 10^{-2}$ cm s^{-1}) samples, with a slightly lower permeability for the film containing a larger amount of organo-functional groups. This can be due to the higher hydrophobicity of such films inducing more resistance to mass transfer from the solution to the electrode surface.

4. Conclusion

Thiol-functionalized porous clay heterostructures have been successfully prepared in one step by self-assembly co-condensation of MPTMS and TEOS, at various MPTMS/TEOS ratios, in the interlayer region of a natural smectite clay. Several physicochemical techniques have been applied to point out the regular structure at the mesoporous level, which was found to decrease slowly by increasing the functionalization degree, and to demonstrate the effective incorporation of mercaptopropyl groups in the final materials. The accessibility to the active sites in these porous solids, as characterized by the uptake of mercury(II) species chosen as a model guest, was found to be very high and gave rise to sorption capacities much higher than unmodified clays or mercaptopropyl-grafted PCHs. Also, mass transfer rates through these highly porous materials were usually fast, especially in the more ordered materials, with however some limitations at pH 2 due to unfavorable electrostatic interactions. An attractive feature of these materials relies on their layered morphology enabling the formation of mechanically stable thin films contrarily to coatings from powdered mesoporous organosilica. Such PCH films were highly permeable in comparison to the nontemplated clays, as checked by hydrodynamic voltammetry, making the functionalized PCHs attractive electrode modifiers likely to enhance the sensitivity of conventional clay-modified electrodes.

Acknowledgment. The work was supported by the French Ministry of Foreign Affairs (program CORUS No. 02 412 043) and the Academy of Science for the Developing World (TWAS Research Unit grant no. 07-052LDC/CHE/AF/AC). The authors are also grateful to J.-P. Emeraux for obtaining XRD patterns, to B. Lebeau and Anne-Catherine Faust for NMR measurements and BET analyses, and to M. Etienne for fruitful discussions.

Supporting Information Available: Figures A−C. This material is available free of charge via the Internet at http://pubs.acs.org.